Porous polymer fibers for low-loss Terahertz guiding

Alireza Hassani, Alexandre Dupuis, Maksim Skorobogatiy

Engineering Physics Department, École Polytechnique de Montréal, C.P. 6079, succ. Centre-Ville Montreal, Québec H3C3A7, Canada

www.photonics.phys.polymtl.ca

Abstract: We propose two designs of effectively single mode porous polymer fibers for low-loss guiding of terahertz radiation. First, we present a fiber of several wavelengths in diameter containing an array of sub-wavelength holes separated by sub-wavelength material veins. Second, we detail a large diameter hollow core photonic bandgap Bragg fiber made of solid film layers suspended in air by a network of circular bridges. Numerical simulations of radiation, absorption and bending losses are presented; strategies for the experimental realization of both fibers are suggested. Emphasis is put on the optimization of the fiber geometries to increase the fraction of power guided in the air inside of the fiber, thereby alleviating the effects of material absorption and interaction with the environment. Total fiber loss of less than 10 dB/m, bending radii as tight as 3 cm, and fiber bandwidth of ~ 1 THz is predicted for the porous fibers with sub-wavelength holes. Performance of this fiber type is also compared to that of the equivalent sub-wavelength rod-in-the-air fiber with a conclusion that suggested porous fibers outperform considerably the rod-in-the-air fiber designs. For the porous Bragg fibers total loss of less than 5 dB/m, bending radii as tight as 12 cm, and fiber bandwidth of ~ 0.1 THz are predicted. Coupling to the surface states of a multilayer reflector facilitated by the material bridges is determined as primary mechanism responsible for the reduction of the bandwidth of a porous Bragg fiber. In all the simulations, polymer fiber material is assumed to be Teflon with bulk absorption loss of 130 dB/m.

OCIS codes: (060.2280) Fiber design and fabrication; (060.4005) Microstructured fibers; (060.5295) Photonic crystal fibers; (230.1480) Bragg reflectors; (999.9999) Terahertz optics.

References and links

1. J. Xu, K.W. Plaxco, S.J. Allen, "Probing the collective vibrational dynamics of a protein in liquid water by terahertz absorption spectroscopy", Protein Sci. **15**, 1175-1181 (2006).
2. D.J. Cook, B.K. Decker, M.G. Allen, "Quantitative THz Spectroscopy of Explosive Materials," OSA conf.: Optical Terahertz Science and Technology, PSI-SR-1196 (2005).
3. C.J. Strachan, P.F. Taday, D.A. Newnham, K.C. Gordon, J.A. Zeitler, M. Pepper, T. Rades, "Using Terahertz Pulsed Spectroscopy to Quantify Pharmaceutical Polymorphism and Crystallinity," J. Pharmaceutical Sci. **94**, 837-846 (2005).
4. M. Nagel, P.H. Bolivar, M. Brucherseifer, H. Kurz, A. Bosserhoff, R. Bttner, "Integrated THz technology for label-free genetic diagnostics," Appl. Phys. Lett. **80**, 154-156 (2002).

#92177 - $15.00 USD Received 28 Jan 2008; revised 8 Apr 2008; accepted 10 Apr 2008; published 21 Apr 2008

5. W.L. Chan, J. Deibel, D.M. Mittleman, "Imaging with terahertz radiation," Rep. Prog. Phys. **70**, 1325-1379 (2007).
6. T. Kiwa, M. Tonouchi, M. Yamashita, and K. Kawase, "Laser terahertz-emission microscope for inspecting electrical faults in integrated circuits," Opt. Lett. **28**, 2058-2060 (2003).
7. K. Kawase, Y. Ogawa, Y. Watanabe, H. Inoue, "Non-destructive terahertz imaging of illicit drugs using spectral fingerprints," Opt. Express **11**, 2549-2554 (2003).
8. T. Lffler, T. Bauer, K.J. Siebert, H.G. Roskos, A. Fitzgerald, S. Czasch, "Terahertz dark-field imaging of biomedical tissue," Opt. Express **9**, 616-621 (2001).
9. G. Gallot, S.P. Jamison, R.W. McGowan, D. Grischkowsky, "Terahertz waveguides," J. Opt. Soc. Am. B **17**, 851-863 (2000).
10. J.A. Harrington, R. George, P. Pedersen, E. Mueller, "Hollow polycarbonate waveguides with inner Cu coatings for delivery of terahertz radiation," Opt. Express **12**, 5263-5268 (2004).
11. C. Themistos, B.M.A. Rahman, M. Rajarajan, K.T.V. Grattan, B. Bowden, J. A. Harrington, "Characterization of silver/polystyrene (PS)-coated hollow glass waveguides at THz frequency," J. Lightwave Technol. **25**, 2456-2462 (2007).
12. C.T. Ito, Y. Matsuura, M. Miyagi, H. Minamide, H. Ito, "Flexible terahertz fiber optics with low bend-induced losses," J. Opt. Soc. Am. B **24**, 1230-1235 (2007).
13. K. Wang, D.M. Mittleman, "Metal wires for terahertz wave guiding," Nature **432**, 376-379 (2004).
14. Q. Cao, J. Jahns "Azimuthally polarized surface plasmons as effective terahertz waveguides," Opt. Express **13**, 511-518 (2005).
15. T. Hidaka, H. Minamide, H. Ito, J. Nishizawa, K. Tamura, S. Ichikawa, "Ferroelectric PVDF cladding terahertz waveguide," J. Lightwave Technol. **23**, 2469-2473 (2005).
16. M. Skorobogatiy, A. Dupuis, "Ferroelectric all-polymer hollow Bragg fibers for terahertz guidance," Appl. Phys. Lett. **90**, 113514 (2007).
17. R.-J. Yu, Y.-Q. Zhang, B. Zhang, C.-R. Wang, C.-Q. Wu, "New cobweb-structure hollow Bragg optical fibers," Optoelectronics Lett. **3**, 10-13 (2007).
18. F. Poli, M. Foroni, D. Giovanelli, A. Cucinotta, S. Selleri, J.B. Jensen, J. Laegsgaard, A. Bjarklev, G. Vienne, C. Jakobsen, J. Broeng, "Silica bridge impact on hollow-core Bragg fiber transmission properties," Proceedings OFC/NFOEC, 1-3 (2007).
19. H. Park, M. Cho, J. Kim, H. Han, "Terahertz pulse transmission in plastic photonic crystal fibres", Phys. Med. Biol. **43**, 3765-3769 (2002).
20. M. Goto, A. Quema, H. Takahashi, S. Ono, N. Sarukura, "Teflon photonic crystal fiber as terahertz waveguide," Jap. J. Appl. Phys. **43**, 317-319 (2004).
21. S.P. Jamison, R.W. McGowan, D. Grischkowsky, "Single-mode waveguide propagation and reshaping of sub-ps terahertz pulses in sapphire fibers," Appl. Phys. Lett. **76**, 1987-1989 (2000).
22. L.-J. Chen, H.-W. Chen, T.-F. Kao, J.-Y. Lu, C.-K. Sun, "Low-loss subwavelength plastic fiber for terahertz waveguiding," Opt. Lett. **31**, 306-308 (2006).
23. M. Nagel, A. Marchewka, H. Kurz, "Low-index discontinuity terahertz waveguides," Opt. Express **14**, 9944-9954 (2006).
24. A. Hassani, A. Dupuis, and M. Skorobogatiy, "Low Loss Porous Terahertz Fibers Containing Multiple Subwavelength Holes," Appl. Phys. Lett **92**, 071101 (2008).
25. A.W. Snyder and J.D. Love, "Optical Waveguide Theory," Chapman Hall, New York, (1983).
26. M.D. Nielsen, N.A. Mortensen, M. Albertsen, J.R. Folkenberg, A. Bjarklev, D. Bonacinni, "Predicting macrobending loss for large-mode area photonic crystal fibers," Opt. Express **12**, 1775-1779 (2004).
27. N.A. Mortensen, "Effective area of photonic crystal fibers," Opt. Express **10**, 341-348 (2002).
28. S.G. Johnson, M. Ibanescu, M. Skorobogatiy, O. Weiseberg, T.D. Engeness, M. Soljacic, S.A. Jacobs, J.D. Joannopoulos, and Y. Fink, "Low-Loss Asymptotically Single-Mode Propagation in Large Core OmniGuide Fibers," Opt. Express **9**, 748 (2001).
29. M. Skorobogatiy, S.A. Jacobs, S.G. Johnson, and Y. Fink, "Geometric variations in high index-contrast waveguides, coupled mode theory in curvilinear coordinates," Opt. Express **10**, 1227-1243 (2002).

1. Introduction

Terahertz radiation, with wavelengths from 30 to 3000 microns, has big potential for applications such as biomedical sensing, noninvasive imaging and spectroscopy. On one hand, the rich spectrum of THz spectroscopy has allowed for the study and label-free detection of proteins [1], explosives [2], pharmaceutical durgs [3], and the hybridization of DNA [4]. On the other hand, the substantial subsurface penetration of terahertz wavelengths has driven a large amount of work on THz imaging [5]. Applications range from non-destructive quality control of electronic circuits [6] to the spatial mapping of specific organic compounds for security

#92177 - $15.00 USD Received 28 Jan 2008; revised 8 Apr 2008; accepted 10 Apr 2008; published 21 Apr 2008

applications [7]. Although THz radiation is strongly absorbed by water, the combination of spectroscopy and imaging has been used to demonstrate the differentiation of biological tissues [8]. Terahertz sources are generally bulky and designing efficient THz waveguides, in order to remotely deliver the broadband THz radiation, would be a big step towards commercialization of compact and robust THz systems. However, almost all materials are highly absorbent in the THz region making design of low loss waveguides challenging. Even air might exhibit high absorption loss if the water vapor content in it is not controlled. Before discussing porous fiber designs, we begin with a review of the recent advances in THz waveguides.

Whereas the losses of circular metallic tubes [9], like stainless steel hypodermic needles, have a propagation loss on the order of 500 dB/m, recent techniques have considerably reduced the loss. On one hand, the use of thin metal layers on the inner surface of dielectric tubes [10, 11, 12], a technique which was initially developed for guiding CO_2 laser light, has been shown to successfully guide in the THz region. A thin Cu layer in a polystyrene tube10 and a thin Ag layer in a silica tube [12] have respectively been shown to have losses of 3.9 dB/m and 8.5 dB/m. On the other hand, surface plasmon mediated guidance on metallic wires has recently raised interest [13] because of the lowest predicted propagation losses [14] of 0.9 dB/m. However, it is very difficult to excite the plasmons because their azimuthal polarization. Typical coupling losses are very high with less than 1% of the incident power transmitted; even with the development of specialized antennas only 50% coupling is achieved. Furthermore, the bending losses are very high and the surface plasmon is a very delocalized mode [14]. Since the mode extends many times the diameter of the wire into the ambient air, modes of these waveguides are expected to couple strongly to the cladding environment. For higher coupling efficiency, and highly confined mode, hollow core waveguides are preferable. As an additional advantage, hollow waveguides offer the possibility of putting an analyte directly into the waveguide core, thus dramatically increasing sensitivity in spectroscopic and sensor applications.

Because of the high absorption losses in dielectrics, a variety of guiding mechanisms have been studied in order to reduce the propagation losses. On one hand, the resonance in the dielectric constant of ferroelectric polyvinylidene fluoride (PVDF) has been exploited for demonstrating a hollow core $n_{core} < 1$ waveguide and a hollow core Bragg fiber [15, 16] with losses lower than 10 dB/m. However, PVDF is a semi-crystalline polymer that has many phases and a complicated poling procedure is required for achieving the ferroelectric state. Another hollow core design was discussed by Yu et al. [17] is of a hollow Bragg fiber where solid layers are separated by air and supported by a network of solid supports, similarly to the air/silica Bragg fibers for the near-IR applications described in [18]. Other photonic crystal structures have been tried [19, 20], but the absorption in a solid core remains considerable.

In yet another approach, many sub-wavelength waveguides have been developed [21, 22, 23]. A solid sub-wavelength rod acts as a high refractive index core with surrounding air acting as a lower refractive index cladding. The field of the guided mode extends far into the surrounding air resulting in low absorption loss. Main disadvantage of rod-in-the-air subwavelength designs is that most of the power is propagated outside of the waveguide core, thus resulting in strong coupling to the environment, which is typically unwanted in power guiding applications. Alternatively, Nagel et al. [23] have demonstrated that addition of a sub-wavelength hole within a solid core increases the guided field within the air hole, thus reducing the absorption losses. Main disadvantage of a subwavelength hole design is that most of the power is still conducted in the high loss material of a core.

While losses of all-dielectric fibers are currently higher than those of hollow core metallized fibers, we believe that porous fiber geometry of a relatively large diameter could be designed to compete with the hollow metallized fibers. The driving factor for the development of porous all-dielectric fibers is that such fibers can be fabricated from a single material using standard fiber

#92177 - $15.00 USD Received 28 Jan 2008; revised 8 Apr 2008; accepted 10 Apr 2008; published 21 Apr 2008

drawing techniques, which is, potentially, simpler than fabrication of metal coated waveguides due to omission of a coating step.

In this paper we present two designs of highly porous fibers that rely on two different guiding mechanisms – the total internal reflection (TIR) and photonic bandgap (PBG) guidance. The geometries of these structures are optimized to increase the fraction of power guided in the air inside of a fiber, thereby reducing the absorption losses and interaction with the environment. The paper is organized as follows. We first present a TIR guiding sub-wavelength fiber containing multiple sub-wavelength holes (see Fig. 1(a)), and compare its performance with that of a subwavelength rod-in-the-air fiber. We then present a PBG guiding porous Bragg fiber (see Fig. 1(b)) featuring a periodic array of concentric material layers separated by air, and supported with a network of circular bridges. Finally we conclude with a summary of the findings.

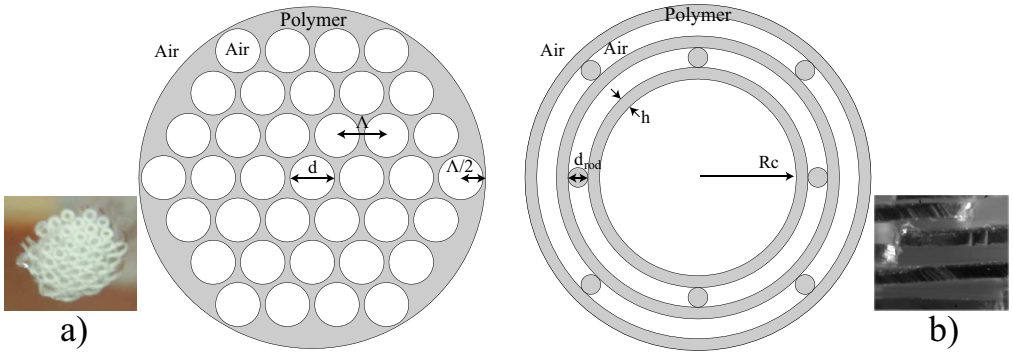

Fig. 1. Schematics of two porous fibers studied in this paper. a) Cross-section of a porous fiber with multiple sub-wavelength holes of diameter $d \ll \lambda$ separated by pitch Λ. b) Cross-section of a porous Bragg fiber featuring periodic sequence of concentric material rings of thickness h suspended in air by a network of circular bridges of diameter d_{rod}.

2. Porous fibers with multiple sub-wavelength holes

We start by reminding the reader briefly the optical properties of porous TIR fibers which were recently detailed in [24]. Our goal is to then perform a comprehensive comparative analysis of TIR porous fibers, sub-wavelength rod fibers, and porous TIR and photonic band gap Bragg fibers - all the excellent candidates for low loss guiding in THz regime.

The first structure we consider consists of a polymer rod having a hexagonal array of air holes (see Fig. 1(a)). Note that a periodic array of holes is not necessary as the guiding mechanism remains total internal reflection and not the photonic bandgap effect. The main task is to design a fiber having a relatively large core diameter for efficient light coupling, while at the same time having a significant fraction of light inside of the fiber air holes to reduce losses due to absorption of a fiber material, as well as to reduce interaction with the environment. In all the simulations presented in this section porous fiber is single mode. Experimentally, such porous fibers can be realized by capillary stacking and drawing technique (see an inset of Fig. 1(a)).

For the fiber material we assume a polymer of refractive index $n_{mat} = 1.5$, which is a typical value for most polymers at 1 THz. Refractive index of air is 1. First, we consider the fiber having 4 layers of subwavelength holes of two possible sizes $d/\lambda = [0.1, 0.15]$, where d is the hole diameter and λ is the operating wavelength. Center-to-center distance between the two holes (lattice pitch) is defined as Λ. Finally, fiber diameter is considered to be 9Λ. In the

#92177 - $15.00 USD Received 28 Jan 2008; revised 8 Apr 2008; accepted 10 Apr 2008; published 21 Apr 2008

remainder of this section the air hole size is fixed for each design, while the thickness of the material veins is varied (larger d/Λ ratios correspond to thinner veins). Fully vectorial finite element method is used for the calculation of the eigen modes of a fiber. In our simulations, design wavelength is fixed $\lambda = 300\ \mu$m (frequency of 1 THz), unless specified otherwise.

Figure 2 shows effective refractive index of the fundamental mode of a porous fiber versus d/Λ for the three cases $d/\lambda = [0.1, 0.15]$. When material vein thickness is reduced (larger d/Λ fractions), effective refractive index of the fundamental mode becomes much smaller than that of a polymer fiber material. As a result, a large fraction of the modal power is expelled into the sub-wavelength air holes and air cladding. Consider, in particular, the case of $d/\lambda = 0.1$. When reducing the vein thickness to 0 ($d/\Lambda \to 1$) from Fig. 2(a) we see that modal effective refractive index monotonically decreases until it saturates at a value ~ 1.045. This saturation happens as even in the case of zero vein thickness the fiber crossection features a network of disjointed, however, finite sized triangular shaped regions.

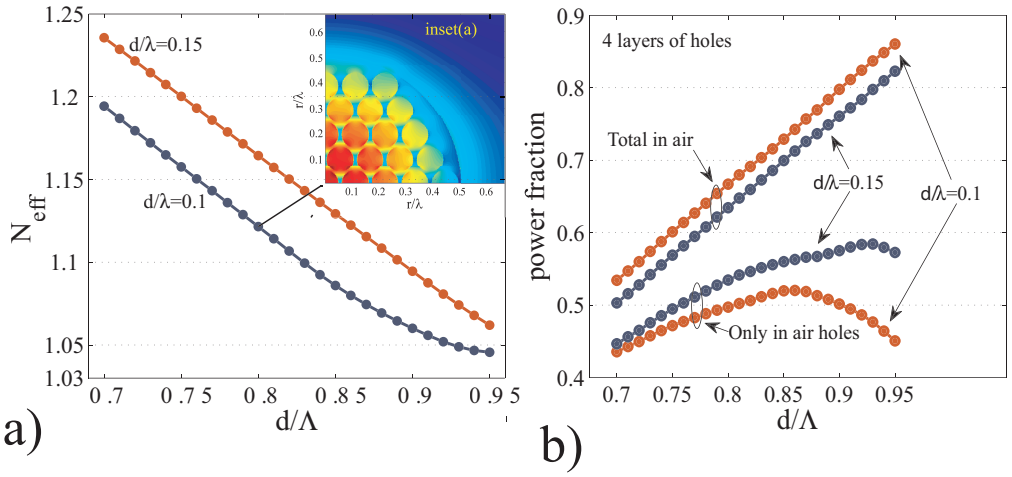

Fig. 2. a) Effective refractive index of the fundamental core mode versus d/Λ for the two fiber designs having hole diameters of $d/\lambda = [0.1, 0.15]$. For the fiber with $d/\lambda = 0.1$, distribution of the power flux in the waveguide crossection Sz is shown for $d/\Lambda = 0.8$ in the inset (a). b) Fraction of modal power guided in the air as a function of d/Λ. The two upper curves show the total power fraction in the air (air plus cladding) while the two lower curves indicate the power fraction in the air holes only.

Insets (a) in Fig. 2(a) shows distributions of the power flux S_z in the fiber crossection for a design with $d/\lambda = 0.1$, and $d/\Lambda = 0.8$. As seen form the inset, the flux distribution has Gaussian-like envelope. As material veins in the case of $d/\Lambda = 0.8$ are very thin, it is not surprising to find that for this design a larger portion of the modal power is concentrated in the air holes. The fraction of power η guided in the air can be obtained by using distribution of the Pointing vector component S_z over the fiber crossection as:

$$\begin{array}{c} \eta = \int_{\text{air}} \mathrm{S_z} dA \Big/ \int_{\text{total}} \mathrm{S_z} dA \\ \mathrm{S_z} \propto Re\left(\hat{z} \cdot \int_{\text{total}} dA\, E \times H^*\right) \end{array} , \tag{1}$$

where "air" and "total" indicate integration over the air regions and the entire fiber cross-section, respectively, while E, H are the modal electric and magnetic fields. Fig. 2(b) shows

#92177 - $15.00 USD Received 28 Jan 2008; revised 8 Apr 2008; accepted 10 Apr 2008; published 21 Apr 2008

the fraction of power guided in the air as a function of d/Λ for the two fibers with different air hole sizes. The two upper curves show the total power fraction in the air (air plus cladding), while the two lower curves indicate the fraction of power contained solely within the air holes. Consider now a particular case of $d/\lambda = 0.1$. As seeing from Fig. 2(b), as the pitch decreases (veins become thinner) the total modal power fraction in the air increases. The power fraction in the air holes inside of the fiber, however, achieves its maximum value at $d/\Lambda \simeq 0.86$. This behavior is relatively simple to rationalize. Indeed, thinning of the material veins beyond their optimal size leads to the reduction of the modal effective refractive index and stronger expulsion of the modal fields into the fiber air cladding, eventually resulting in the smaller modal power fraction in the air holes of a fiber core. On the other hand, thickening of the material veins beyond their optimal size leads to higher concentration of the modal fields inside of the polymer veins, eventually also resulting in the smaller modal power fraction in the air holes of a fiber core. From Fig. 2(b) it follows that for a given size of the air holes d/λ, the d/Λ parameter can be optimized to increase the amount of power propagating inside of the porous fiber core, thus reducing the influence of cladding environment. Inversely, if the d/Λ is fixed, the air hole size d/λ can be also optimized to increase the amount of power propagating inside of the porous fiber. For the reference, existence of an optimal air hole size to maximize the fraction of power guided in the air was first described in the case of a single sub-wavelength air hole inside of a solid core waveguide [23].

We now characterize absorption loss of the fundamental mode due to fiber material absorption. Particularly, the ratio of the modal absorption loss to the bulk material loss of a core material can be calculated using perturbation theory expression [25]:

$$f = \frac{\alpha_{\text{mode}}}{\alpha_{\text{mat}}} = \frac{Re(n_{\text{mat}}) \int_{\text{mat}} |E|^2 dA}{Re\,(\hat{z} \cdot \int_{\text{total}} dA\, E \times H^*)}, \tag{2}$$

where α_{mat} is the bulk absorption losses of the core material (assuming that air has no loss). Figure 3(a) presents the normalized absorption loss of the fundamental core mode as a function of d/Λ. Not surprisingly, for higher air filling fractions (larger d/Λ) absorption loss is greatly reduced. For example, for a fiber with $d/\lambda = 0.1$, $d/\Lambda = 0.95$ the normalized absorption loss is ~ 0.08. Considering that the fiber is made of a low loss polymer such as Teflon [20] with bulk absorption loss of $\alpha_{mat} = 0.3\,\text{cm}^{-1} \simeq 130\,\text{dB/m}$ at 1 THz we obtain the fundamental mode loss $\alpha_{\text{mode}} = 10.4\,\text{dB/m}$.

Another important parameter to consider is radiation loss due to macrobending. In general, calculation of bending induced loss for microstructured fibers is not an easy task. In our case, however, due to Gaussian like envelope of the fundamental mode we can approximate our fiber as a low refractive index-contrast step-index fiber for which analytical approximation of bending loss is readily available [26]:

$$\alpha \cong \frac{\sqrt{\pi}}{8} \frac{1}{A_{eff}} \frac{1}{\beta(\beta^2 - \beta_{\text{cl}}^2)^{1/4}} \frac{\exp\left(-\frac{2}{3} R_b (\beta^2 - \beta_{\text{cl}}^2)^{3/2} \beta^{-2}\right)}{\sqrt{R_b(\beta^2 - \beta_{\text{cl}}^2)\beta^{-2} + R_c}} \propto \frac{1}{\sqrt{\lambda R_b}} \exp(-\frac{R_b}{\lambda} \cdot const), \tag{3}$$

where modal propagation constant β is defined as $\beta = 2\pi n_{eff}/\lambda$, R_b is bending radius, R_c is a fiber core radius, and A_{eff} is the modal effective area defined as [27]:

$$A_{\text{eff}} = \left[\int I(r) r dr\right]^2 \Big/ \left[\int I^2(r) r dr\right], \tag{4}$$

where $I(r) = |E_t|^2$ is the transverse electric field intensity distribution in the fiber crossection. As an example, consider porous fiber having $d/\lambda = 0.1$, and operated at $\lambda = 600\,\mu\text{m}$

#92177 - $15.00 USD Received 28 Jan 2008; revised 8 Apr 2008; accepted 10 Apr 2008; published 21 Apr 2008

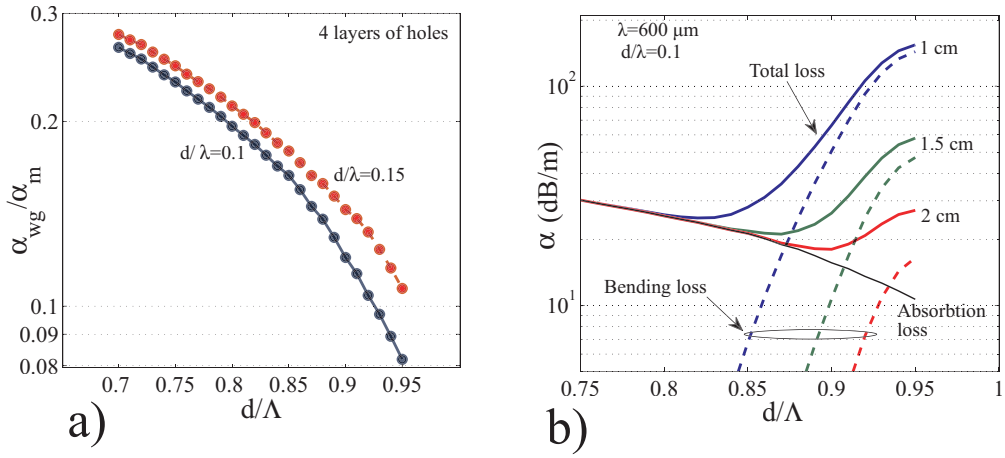

Fig. 3. a) Normalized absorption loss versus d/Λ for two porous fiber designs. b) Total of the bending and absorption losses versus d/Λ for the Teflon-based porous fiber with $d/\lambda = 0.1$ operating at 0.5 THz.

(0.5 THz)(the longer operating wavelength, $\lambda = 600\,\mu$m, shows a more challenging case for bending loss). In Fig. 3(b) we compare absorption, bending and total modal losses as a function of d/Λ design parameter. Thin solid curve represents straight fiber absorption loss assuming that the fiber is made of a Teflon polymer having 130 dB/m bulk absorption loss. Dashed curves show fiber macro-bending loss calculated using (3) for 1 cm, 1.5 cm, and 2 cm values of the bending radii R_b. Finally, thick solid curves present total modal loss (the sum of absorption and bending losses). Interestingly, for very tight bends (bending radii of several cm and smaller) there exists an optimal design (in terms of d/Λ) that minimizes the total loss. Generally, for moderate air filling fractions $0.8 < d/\Lambda < 0.9$ the dominant loss mechanism is absorption loss due to field localization in the material core, whereas for high air filling fractions $d/\Lambda > 0.85$ bending loss dominates due to strong delocalization of the fundamental mode outside of the fiber core.

We conclude this section by comparing performance of a 3 layer porous fiber [18](with reducing one layers of holes) with that of a standard rod-in-the-air sub-wavelength fiber made of the same material (see Fig. 4). To make a fair comparison, we first design a rod-in-the-air fiber having the same absorption losses as a porous fiber, and then compare various propagation characteristics of the two fibers. Particularly, we consider porous fiber of Fig. 1(a) with $d/\lambda = 0.1$, $\lambda = 300\mu m$. For every value of $0.7 < d/\Lambda < 0.95$ of a porous fiber, we then find a corresponding diameter D_r of a rod-in-the-air fiber so that the absorption losses of the two fibers are identical. For both fibers the core material is assumed to be Teflon polymer with $n_{mat} = 1.5$ and bulk absorption loss $\alpha_{mat} = 130$ dB/m. In Fig. 4(a) we first compare normalized diameters of the two fibers and observe that the core diameter of a rod-in-the-air fiber has to be significantly smaller than that of a porous fiber to achieve the same absorption loss. When comparing the effective modal diameters of the fundamental modes one notices that for a porous fiber the modal diameter is comparable to the size of a fiber core, while for a rod-in-the-air fiber the modal diameter is considerably larger than that of a fiber core. In other words, fundamental mode of a porous fiber is considerably less sensitive to the changes in the air cladding environment than the fundamental mode of a rod-in-the-air fiber. Superior field confinement by the porous fiber is also responsible for the higher effective refractive index of the fundamental mode of a porous fiber compared to that fiber compared to that of a rod-in-the-air fiber (see Fig. 4(b)). Finally,

#92177 - $15.00 USD Received 28 Jan 2008; revised 8 Apr 2008; accepted 10 Apr 2008; published 21 Apr 2008

we compare bending losses of the two fibers in Fig. 4(c). Using expression (3) we calculate and plot bending losses of the 3 layer porous fiber for the three different values of a fiber bending radius $R_b = [0.5\text{cm}, 1.0\text{cm}, 1.5\text{cm}]$, as well as bending losses of a rod-in-the-air fiber for $R_b = [1.0\text{cm}, 4.0\text{cm}, 7.5\text{cm}]$. We observe that for two fibers having the same absorption losses to also have similar bending losses, the bending radius of a rod-in-the-air fiber has to be significantly larger than a bending radius of a porous fiber. This makes us to conclude that resistance of a porous fiber to bending is superior to that of a rod-in-the-air fiber.

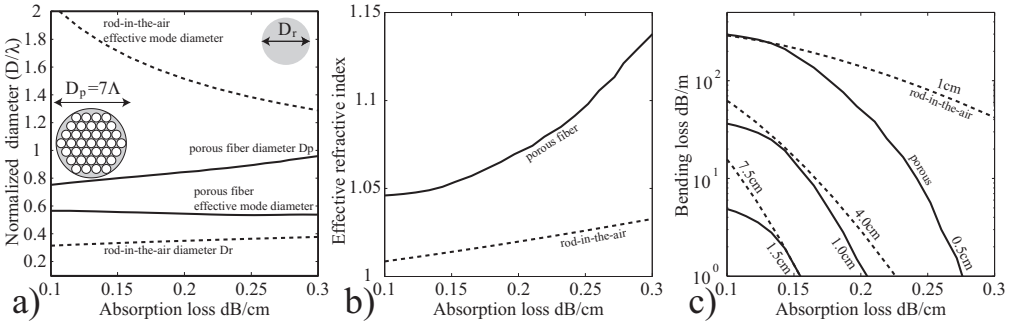

Fig. 4. Comparison of the propagation characteristics of the fundamental mode of a porous fiber (solid curves) with those of the fundamental mode of the equivalent rod-in-the-air subwavelength fiber (dashed curves). a) Normalized fiber and mode diameters. b) Modal effective refractive indices. c) Modal losses due to macro-bending.

Finally, we comment on the overall size of a porous single mode fiber featuring N layers of holes. As follows from the schematic of Fig. 1(a), the diameter of a porous fiber is:

$$D_p = (2N+1)\,\Lambda = \lambda\left[(2N+1)\,(d/\lambda)\,/\,(d/\Lambda)\right] \approx \lambda\,(2N+1)\,(d/\lambda)\,. \tag{5}$$

In (5) we have used the fact that in most designs the vein thickness is small $d/\Lambda \approx 1$. Particularly, in the case of $N = 3$ layers of holes and $d/\lambda \approx 0.1 - 0.2$ considered in this section we get $D_p \approx \lambda$; although the fiber diameter is not sub-wavelength, it is, however, comparable to the wavelength of operation. To simplify coupling to a THz beam of a typical diameter of $5 - 10$ mm it is desirable to explore the possibility of designing single mode porous fiber with a diameter which is, at least, several times larger than the wavelength of operation. As follows from (5), one way of achieving this goal is by increasing the number of layers of holes in the fiber (see Fig. 5(a)), which also results in modes with larger effective areas. When increasing the fiber diameter, one has to be careful to ensure that the fiber remains single mode. Therefore, once the number of layers is increased, one typically has to make the material veins thinner. Unfortunately, our FEM software did not allow us to investigate fibers with more than $N = 5$ layers of holes. To demonstrate the possibility of large core-diameter porous fibers we resorted to design of porous Bragg fibers (see Fig. 5(b)) for which transfer matrix approach [28] allows treatment of much larger systems. Particularly, in Fig. 5(b) we show schematic of a porous Bragg fiber consisting of 13 concentric material layers of thickness $h/\lambda = 0.01$ forming a periodic multilayer with a period Λ. Relative size of the air gap between individual layers is taken to be $(\Lambda - h)/\Lambda = 0.95$. With these parameters such a Bragg fiber is single mode with effective modal diameter of 5λ (mode diameter is comparable to the fiber core radius), and normalized absorption loss is 0.054. Energy flux distribution in the fundamental mode of such a fiber is shown in Fig. 5(b) exhibiting an overall Gaussian-like envelope with a small dip in the center. This demonstrates that, in principle, by increasing the number of periods in a fiber crossection, while reducing the thickness of material layers, one can design large area single mode

#92177 - $15.00 USD Received 28 Jan 2008; revised 8 Apr 2008; accepted 10 Apr 2008; published 21 Apr 2008

porous fibers having most of the field confined in the fiber core and exhibiting greatly reduced absorption loss.

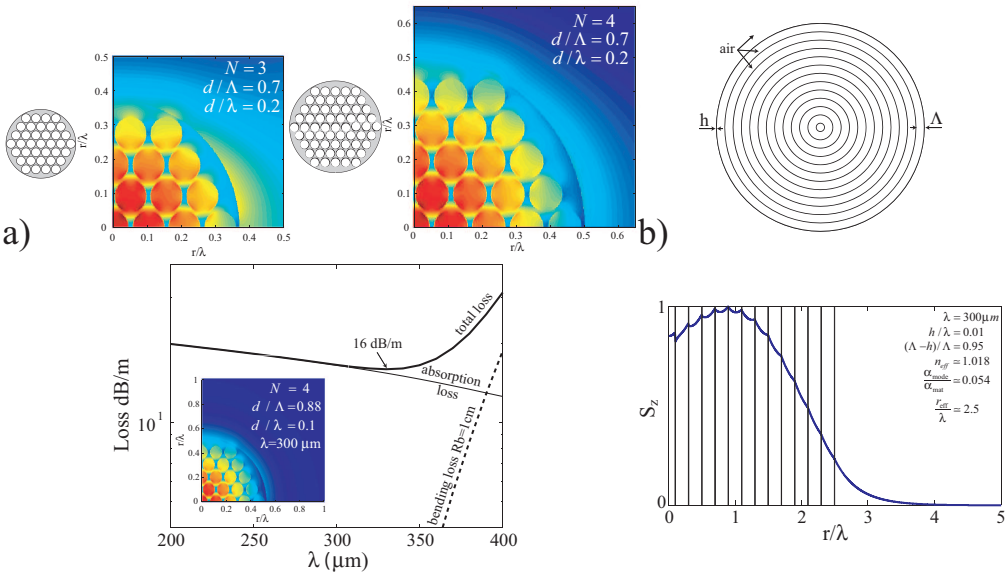

Fig. 5. Various implementations of porous fibers. a) Increasing the number of layers in a porous fiber leads to modes with larger effective mode diameters. In the lower plot a typical performance of a 4 layer porous fiber designed for $\lambda = 300\ \mu$m is shown. b) Schematic of a 25 layer porous Bragg fiber and flux distribution in its fundamental mode.

We conclude this section by presenting performance of a typical porous fiber as a function of the wavelength of operation. The fiber in question is designed for $\lambda = 300\ \mu$m, has 4 layers of holes, and is characterized by $d/\lambda = 0.1$, $d/\Lambda = 0.88$. Fiber diameter is $D \simeq \lambda$. The material of the fiber is assumed to be Teflon polymer with bulk material loss $\alpha_{mat} = 130$ dB/m. In Fig. 5(a) we demonstrate absorption and bending losses of such a fiber assuming a very tight $R_b = 1$ cm bending radius. The fiber is effectively insensitive to bending as bending loss stays much smaller than the absorption loss even for very tight bending radii. We also see that performance of this fiber is broadband with total propagation loss less than 20 dB/cm across the whole $200 - 400\ \mu$m wavelength region assuming the presence of bends as tight as $R_b = 1$ cm.

3. Porous photonic bandgap Bragg fibers with a network of bridges

In the remainder of the paper, we analyze guiding of THz radiation using porous photonic bandgap Bragg fiber. Schematic of such a fiber is shown in Fig. 1(b); Bragg fiber consists of a sequence of concentric material layers suspended in air by a network of material bridges in the shape of sub-wavelength rods. For the reference, porous Bragg fiber geometry was recently discussed by Yu et al. [17], where instead of rods, thin material bridges were proposed, however, practical implementation of such a geometry may be challenging. Analysis of transmission properties of the air/silica based Bragg fibers with bridges for near IR applications was also presented recently in [18].

As detailed in Fig. 1(b), proposed fiber consists of a sequence of circular material layers of thickness h suspended in air by circular bridges (rods) of diameter d_{rod}. Thickness of the air layers is the same as the diameter of circular bridges. Since the bridges are small, the layers

#92177 - $15.00 USD Received 28 Jan 2008; revised 8 Apr 2008; accepted 10 Apr 2008; published 21 Apr 2008

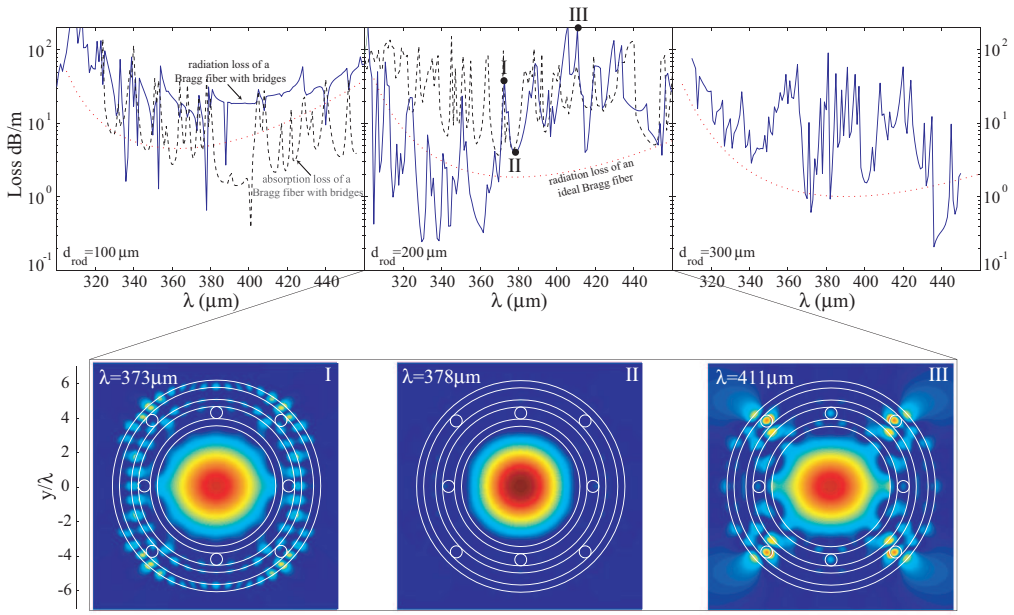

Fig. 6. Radiation losses (solid lines) and absorption losses (dashed lines) of the hollow core Bragg fibers for various bridge sizes $d_{rod} = [100, 200, 300]$ μm. For comparison, radiation loss of the equivalent Bragg fibers without rods are presented as dotted lines. Inset II shows S_z flux distribution in the fundamental core guided mode positioned at the minimum of the local bandgap at $\lambda = 378$ μm. Insets I and III show field distributions in the fundamental core mode at the wavelengths of coupling with different surface states.

containing the bridges have an effective index close to that of air. Thus, the alternating layers of polymer and air yield a high index-contrast Bragg fiber. Core radius R_c of a hollow Bragg fiber is assumed to be considerably larger than the wavelength of propagating light. Guidance in the hollow core is enabled by the photonic bandgap of a multilayer reflector. In the ideal Bragg fiber without bridges, for a design wavelength λ_c to coincide with the center of a photonic bangap of a multilayer reflector, thicknesses of the material and air layers have to be chosen to satisfy the following relation [16]:

$$d_{rod}\sqrt{n_{air}^2 - n_{eff}^2} + h\sqrt{n_{mat}^2 - n_{eff}^2} = \lambda_c/2. \tag{6}$$

Taking into account that in a large hollow core fiber the lowest loss core mode has effective refractive index n_{eff} slightly lower but very close to that of air n_{air}, we conclude that rod size does not affect considerably the resonance condition (6) and, therefore, can be chosen at will, while material layer thickness has to be chosen as $h = \lambda_c \Big/ \left(2\sqrt{n_{mat}^2 - n_{air}^2}\right)$. Note that this choice of material thickness is only an approximation, and therefore one should not expect exact matching of the wavelength of the center of a reflector bandgap with λ_c. In what follows we consider several designs of a 3 layer Bragg fiber with the following parameters $n_{mat} = 1.6$, $n_{air} = 1$, $d_{rod} = [100, 200, 300]$ μm. Design wavelength is $\lambda_c = 300$ μm, leading to the $h = 120$ μm choice of a material layer thickness. Fiber core radius is assumed to be $R_c = 1$ mm $\simeq 3.3\lambda_0$. Finally, fiber material loss is assumed to be comparable to that of a Teflon polymer $\alpha_{mat} = 130$ dB/m.

#92177 - $15.00 USD Received 28 Jan 2008; revised 8 Apr 2008; accepted 10 Apr 2008; published 21 Apr 2008

In Fig. 6 we present radiation losses (solid curves) and absorption losses (dashed curves) of the fundamental HE_{11} core guided mode of a Bragg fiber with bridges for various bridge sizes. For comparison, radiation losses of the fundamental core mode of equivalent Bragg fibers with identical parameters, however, without the dielectric bridges, are shown as dotted curves. Overall, radiation losses of the Bragg fibers with bridges follow radiation losses of the equivalent Bragg fibers without bridges. However, bandgaps of the Bragg fibers with bridges are fractured due to crossing of the core mode dispersion relation with those of the surface states. At the minima of the local bandgaps (see inset II in Fig. 6), field distribution of the fundamental core guided mode is Gaussian-like and it is well confined inside of the hollow core. For example, for $d_{rod} = 200\ \mu$m at $\lambda = 378\ \mu$m the total waveguide loss is ~ 8.7 dB/m and the bandwidth is $\sim 10\ \mu$m. In principal, by adding only few more layers into Bragg reflector (5-7 material layers instead of 3 material layers shown in Fig. 1(b)), radiation loss can be reduced below absorption loss resulting in fibers of ~ 5 dB/m total loss in the case of $d_{rod} = 200\ \mu$m, and fibers of ~ 1 dB/m total loss in the case of $d_{rod} = 100\ \mu$m. At the wavelengths of crossing with surface states (see insets I and III in Fig. 6), radiation and absorption losses increase considerably due to excitation of the highly lossy surface states localized inside of the material layers of a Bragg reflector. As seen from the insets I and II in Fig. 6, fields of the surface states are concentrated in the vicinity, or directly, at the material bridges separating separating concentric layers of a Bragg reflector. By comparing the loss data in Fig. 6 for various fiber designs one concludes that when bridge size increases, the number of surface states also increases. Therefore, to improve fiber bandwidth one has to avoid fracturing of the reflector bandgap with surface states, which is, in principle possible, by reducing the thickness of the bridges. of the bridges. However, even in the best case scenario of ideal Bragg fibers without any bridges, bandwidth of a plastic-based fiber with $n_{mat} \sim 1.6$ is relatively small and on the order of $\sim 100\ \mu$m ~ 0.3 THz.

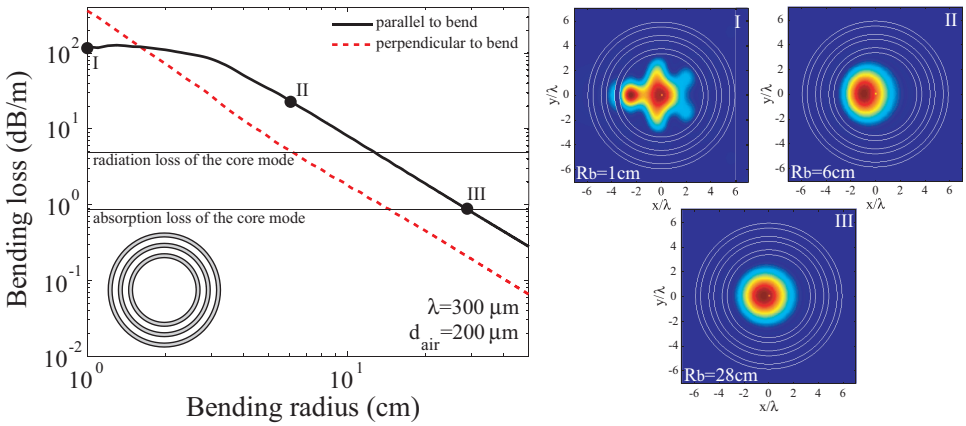

Fig. 7. Bending losses of a porous Bragg fiber without bridges designed and operated at $\lambda_c = 300\ \mu$m. Bending loss is strongly sensitive to the polarization of an HE_{11} mode, with the polarization in the plane of a bend being the lossiest. In the insets we show S_z flux distributions at the output of the 90^0 bends of various radii.

Finally, to evaluate resistance of the porous Bragg fibers to bending, we present macro-bending loss analysis for the case of porous Bragg fibers without bridges. We use perturbation matched coupled-mode theory described in [29] to solve mode scattering problem due to bending, assuming that at the bend input a single HE_{11} mode is excited. Simulated bending losses are presented in Fig. 7 for the two orthogonal modal polarizations (parallel and perpendicular to the plane of the bend). Note that bending loss is strongly polarization dependent, with the

#92177 - $15.00 USD Received 28 Jan 2008; revised 8 Apr 2008; accepted 10 Apr 2008; published 21 Apr 2008

polarization in the plane of a bend being the lossiest. We also note that for the bending loss of the lossiest polarization to be lower than the straight fiber radiation loss one has to insure bending radii of no tighter than 12cm. Fig. 7 we show field distributions at the output of the 90^0 bends of various radii. For tight bending radii $R_b < 6$ cm we observe that not only bending loss becomes appreciable, but also the quality of the output beam deteriorates as judged by the non-Gaussian distribution of the beam fields.

We conclude this section by mentioning in passing that we have attempted fabrication of porous Bragg fibers experimentally. Inset in Fig. 1(b) presents optical microscope image showing a small part of the cross-section of a porous multilayer. The fiber was made by co-rolling of a solid PMMA film with a second PMMA film that had windows cut into it. Once rolled, the windows formed the air gaps and the remaining bridges of the cut film formed bridges separating the solid film layers. Preliminary bolometer measurements of THz transmission through porous Bragg fibers having 1 cm hollow core diameter resulted in total loss estimate of ~ 40 dB/m. We are currently pursuing more detailed transmission measurements of these fibers.

4. Conclusions

We have proposed two types of porous plastic fibers for low-loss guidance of THz radiation. Firstly, a microstructured polymer THz fiber composed of a polymer rod containing hexagonal array of sub-wavelength air holes was discussed. Let us emphasize that a periodic array of holes is not necessary as the guiding mechanism remains total internal reflection, and not the photonic bandgap effect. Although in this design the fiber core diameter is comparable to that of the wavelength of operation, nevertheless, the major portion of THz power launched into the fiber is confined within the air holes inside of the fiber core. As a result, coupling to the cladding environment is greatly reduced, while the modal absorption loss lower than 10 dB/m can be achieved with 130 dB/m bulk absorption loss of a fiber material. Using approximate analytical expression to calculate macro-bending losses, allowed us to conclude that suggested porous fibers are highly resistant to bending, with bending loss being smaller than modal absorption loss for bends as tight as 3 cm of radius. Finally, suggested porous fibers are broadband having ~ 1 THz bandwidth even in the presence of tight bends. Secondly, we have considered porous photonic bandgap Bragg fibers made of a set of concentric material layers suspended in air by the network of circular bridges. Fiber hollow core diameter is much larger that the operating wavelength, thus allowing efficient coupling to various THz sources. Although total modal loss (absorption plus radiation loss) lower than 5 dB/m can be achieved with 130 dB/m bulk absorption loss of a fiber material, fiber bandwidth was found to be smaller than 0.1 THz. Parasitic coupling to the surface states of a multilayer reflector facilitated by the material bridges was determined as primary mechanism responsible for the reduction of the bandwidth of a porous photonic bandgap Bragg fiber.

#92177 - $15.00 USD Received 28 Jan 2008; revised 8 Apr 2008; accepted 10 Apr 2008; published 21 Apr 2008